Biophysical Journal
Article

Biophysical Society

The Limiting Speed of the Bacterial Flagellar Motor

Jasmine A. Nirody,[1,*] Richard M. Berry,[3] and George Oster[2]
[1]Biophysics Graduate Group and [2]Department of Molecular and Cell Biology, University of California, Berkeley, Berkeley, California; and [3]Department of Physics, Clarendon Laboratory, University of Oxford, United Kingdom

ABSTRACT Recent experiments on the bacterial flagellar motor have shown that the structure of this nanomachine, which drives locomotion in a wide range of bacterial species, is more dynamic than previously believed. Specifically, the number of active torque-generating complexes (stators) was shown to vary across applied loads. This finding brings under scrutiny the experimental evidence reporting that limiting (zero-torque) speed is independent of the number of active stators. In this study, we propose that, contrary to previous assumptions, the maximum speed of the motor increases as additional stators are recruited. This result arises from our assumption that stators disengage from the motor for a significant portion of their mechanochemical cycles at low loads. We show that this assumption is consistent with current experimental evidence in chimeric motors, as well as with the requirement that a processive motor driving a large load via an elastic linkage must have a high duty ratio.

INTRODUCTION

The bacterial flagellar motor (BFM) drives swimming in a wide variety of bacterial species, making it crucial for several fundamental biological processes, including chemotaxis and community formation (1–4). Accordingly, gaining a mechanistic understanding of this motor's function has been a fundamental challenge in biophysics.

Because of its complexity and localization to the membrane, atomic structures of the entire motor are not yet available. Still, relatively detailed models have been developed using a combination of partial crystal structures (5–7), cross-linking and mutagenesis (8–10), and electron microscopic and cryoelectron tomography images (11,12) (Fig. 1). Additionally, the relative ease with which the output of a single motor can be measured in real time, by observing rotation of a large bead attached to the motor with light microscopy, has made it one of the best studied of all large biological molecular machines.

Arguably the most important physical probe into the *dynamics* of a molecular motor is its torque-speed relationship. For the BFM, this curve was shown to have two distinct regimes, separated by a "knee" (Fig. 2). This characteristic feature of the BFM was long held as the first "checkpoint" for any theoretical model of the motor. However, recent experiments showed that the number of torque-generating complexes (*stators*) in the motor is load-dependent—that is, published torque-speed curves most likely contain measurements from motors with different numbers of docked stators (13,14). Specifically, at high loads (low speeds) a motor can have up to 11 docked stators, whereas at low loads (high speeds) motors typically operate with only one stator (though we note that the experiments in (13) reported that ~25% of motors likely had two stators).

Before continuing, we first clarify some of our terminology. We consider the "low load" regime (also referred to as "high speed," "maximum speed," or "zero torque" throughout) to be when the drag coefficient of the load is on the same order of magnitude or lower than the internal friction (i.e., the drag of the rotor). Importantly, we point out that due to experimental constraints, several results originally considered to be "low load" measurements were conducted using loads outside of this regime; these will be noted as they appear in our text.

The recent experimental findings (13,14) shed doubt on several fundamental results about the dynamics of the BFM, including, importantly, its behavior at low loads. A seminal set of experiments, termed "resurrection" experiments, studied the dependence of motor speed on the number of stators at various external loads (15–17). In these experiments, paralyzed cells were allowed to begin rotating slowly, and discrete increases in speed were interpreted as the addition of torque-generating complexes. Surprisingly, whereas up to 11 increases of near-equal size were observed at high loads, only a single such "jump" was observed at low loads.

These results quickly led to a series of reworked theoretical models, all of which required that the limiting speed of

Submitted November 23, 2015, and accepted for publication July 5, 2016.
*Correspondence: jnirody@berkeley.edu
Editor: Sean Sun
http://dx.doi.org/10.1016/j.bpj.2016.07.003

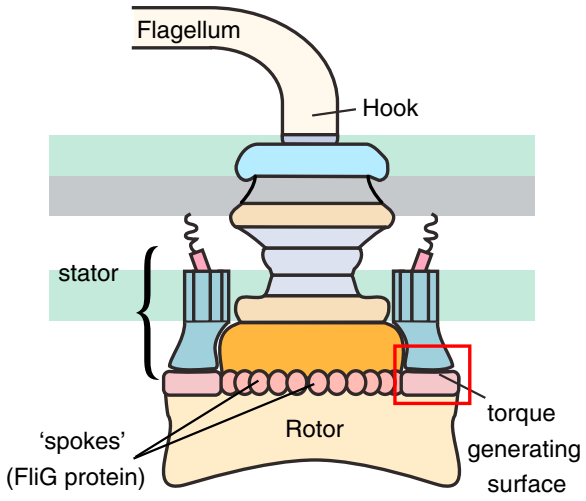

FIGURE 1 The bacterial flagellar motor consists of a series of large concentric rings that attach to a flagellar filament via a flexible hook. An active motor can have between 1 and 11 torque-generating stator complexes. Stators interact with protein "spokes" (FliG) along the rotor's edge to drive motor rotation. To see this figure in color, go online.

the motor be independent of the number of stators (18–20). However, it is likely that low-load measurements were never performed on motors with more than one stator, leaving open the question of how the BFM behaves in the zero-torque (high-speed) limit.

We recently presented a model of flagellar motors with a single stator, in which a steric interaction driven by a conformational change in the stator is implicated as the motor's torque-generating mechanism (21). In this study, we extend this model to motors with multiple-docked stators and predict that the limiting speed of the BFM increases with the number of active stators.

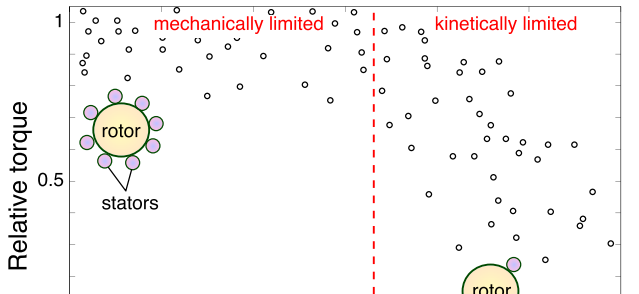

FIGURE 2 Recent experiments have shown that the number of torque-generating complexes (stators) is not constant across applied loads. Therefore, it is likely that most measured torque-speed curves were generated using motors with varying numbers of stators: points in the high-load regime correspond to motors with up to 11 stators and points at low loads (within the kinetically limited regime) to motors with only one. Red dashed line separates the mechanically limited and kinetically limited regimes; we focus on the latter. Data shown is from (46); however, we note that another experiment in this same article presents data that seems to be collected from a motor with a constant number of stators. To see this figure in color, go online.

This result arises from the fact that the stator is not in contact with the rotor in between steps, or "power strokes" (i.e., the *duty ratio* of the motor is less than 1). We note that although models with high duty ratios also can reproduce current experiments, evidence of a conformational change in stator structure has been reported (see, e.g., (22)). Generic models involving such a conformation will share this property, because such mechanisms likely require stators to "reset" between steps.

In the following, we first give an overview of our model for single-stator motors and then discuss its extension to motors with multiple-docked stators. We then discuss the implication of such a model for motors operating at low load: in particular, challenging the widely held belief that the motor speed near the zero-torque limit is independent of the number of docked stators.

We argue that these mechanisms affect the motor's duty ratio only at low loads. In this way, our model, and others in this category, are compatible with evidence that the BFM must have a high duty ratio to be processive at high loads. Experiments testing this hypothesis, if successful, would be the first, to our knowledge, to explicitly quantify this relationship in the low-load regime.

MATERIALS AND METHODS

Our model implicates a steric interaction between the stator and rotor in torque generation (21). Briefly, stators drive motor rotation by stepping along protein "spokes" around the periphery of the rotor, a large ring that connects to the flagellar filament via a flexible hook. This interaction is analogous to parents pushing on the handles of a merry-go-round on the playground for their children's amusement. An overview of our proposed mechanism is given in Fig. 3.

Individual steps are initiated by proton arrivals at ion-binding sites within the stator complex. The gate-controlled diffusion of protons through the BFM's stator, and its link to motor rotation, was recently explored (23). During the power stroke, conformational changes in the stator apply a steric force onto the spokes of the rotor wheel, rotating it a discrete step length d. Details of the stator potential curves are provided in the Supporting Material and in reference (21).

The motion of the stator and rotor are described by the following Langevin equations:

$$\zeta_S \frac{d\phi_S}{dt} = \underbrace{F_p \ell_p}_{\substack{\text{Torque from}\\ \text{Proline hinge}}} - \underbrace{\tau_{\text{reaction}}}_{\substack{\text{Reaction}\\ \text{from rotor}}} + \underbrace{\sqrt{2k_BT\zeta_S} f_n(t)}_{\text{Thermal fluctuations}}$$

$$\zeta_R \frac{d\theta_R}{dt} = \underbrace{\tau_{\text{contact}}}_{\substack{\text{Torque}\\ \text{from stator}}} - \underbrace{\kappa(\theta_R - \theta_L)}_{\substack{\text{Spring connection}\\ \text{to load}}} + \underbrace{\sqrt{2k_BT\zeta_R} f_n(t)}_{\text{Thermal fluctuations}},$$

where the final term in each equation is the stochastic Brownian force, with k_BT being the Boltzmann constant multiplying temperature and $f_n(t)$ denoting uncorrelated white noise.

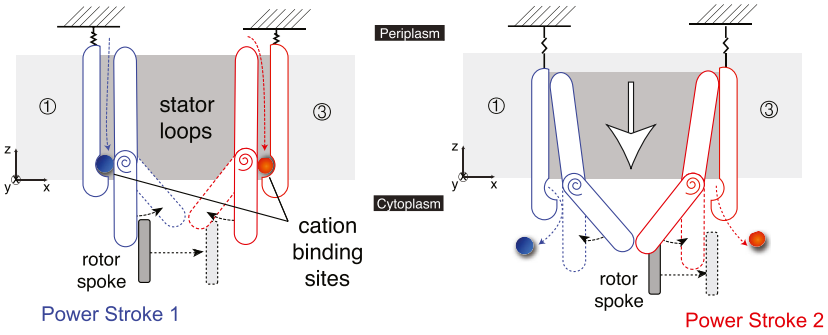

FIGURE 3 Overview of our proposed torque-generating mechanism. Cation binding induces a strain in the stator, which causes the loops to bend. This results in the first half of the power stroke (here, by Loop 1), and sets up the second loop (here, Loop 3) to perform its half of the power stroke. Subsequently, the cations are released into the cytoplasm. This occurs because our proposed motion also has a vertical component—the loops lower themselves out of the membrane. This release then reverses the strain and causes the loops to re-straighten. This results in the second half of the power stroke. We note that this image depicts a two-dimensional projection of a three-dimensional motion: stator motion is not constrained to the plane of the page. To see this figure in color, go online.

Stators apply no force ($F_p = 0$) to the rotor between power strokes. This results in negligible applied (τ_{contact}) and reaction torque (τ_{reaction}) when the stator and rotor are not in contact with each other. The values of these torques are calculated as the gradients of the interaction potential between the stator and the rotor; details on these calculations are provided in the Supporting Material. All other model parameters are described in Table 1. Because the BFM lives at low Reynolds number, the rotor also exhibits no productive movement when the stator is disengaged between steps.

We assumed that there are 26 spokes along the edge of the rotor ((24), although see, e.g., (7,25)). A "perfect" power stroke is defined as a step of length $d = (2\pi/26)$ rad, leaving the stator in contact with the neighboring spoke. These steps are observed through the rotation of a small bead (the load) attached to the flagellar hook. The dynamics of the load are described by a third Langevin equation:

$$\zeta_L \frac{d\theta_L}{dt} = \underbrace{\kappa(\theta_R - \theta_L)}_{\substack{\text{Spring connection} \\ \text{to rotor}}} + \underbrace{\sqrt{2k_B T \zeta_L} f_n(t)}_{\text{Thermal fluctuations}}.$$

When the connection between the rotor and the bead is soft (κ is small), discrete motor steps "blur" into a seemingly continuous trajectory. Experimentally, steps have been directly observed by slowing the motor down to a speed of ~10 Hz (24).

In a motor with multiple stators, the mechanics of each stator follows the equations corresponding to that of a single stator. At any given time, docked stators can be "engaged" (i.e., actively performing a power stroke) or "disengaged" (in between power strokes). The total contact torque on the rotor is given by the following:

$$\tau_{\text{contact}} = \sum_{i=1}^{N} \tau^i_{\text{contact}},$$

where N is the total number of docked stators, and each stator i applies a contact torque τ^i_{contact} on the rotor. Recall that a disengaged stator (i.e., one in the waiting state between successive power strokes) is not applying directional torque to the rotor, and so $\tau^i_{\text{contact}} = 0$.

We have assumed that each stator is independently "activated" with rates corresponding to cation "hopping on" and "hopping off" events. Because cation arrivals are Poisson processes (i.e., waiting times between arrivals are distributed exponentially) (26,27), the "next arrival" in a motor with N stators occurs at a rate $N \times k_{\text{on}}$, where k_{on} is the rate of arrival for a single stator.

Simulations of Langevin dynamics were written in Python 2.7. Further details on the implementation and interaction potentials used in simulations are provided in the Supporting Material. Simulation trajectories showing steps for motors with one and seven engaged stators operating at low load are shown in Fig. 4, *a* and *b*. (All code is available at http://ocf.berkeley.edu/~jnirody)

TABLE 1 Model Parameters with Units, Values, and Reference

Parameter	Definition	Units	Values	References
F_p	Proline hinge force	pN	20	(1)
ℓ_P	Length of proline hinge	nm	7	(44)
ζ_S	Stator drag coefficient	pN-nm-s-rad^{-1}	0.002	fit
ζ_R	Rotor drag coefficient	pN-nm-s-rad^{-1}	0.02	(1)
ζ_L	Load drag coefficient	pN-nm-s-rad^{-1}	0.005–10	(45)
κ	Hook spring constant	pN-nm-rad^{-1}	150	(40)
N	Number of stators	-	1–11	(45)
τ_{contact}	Contact torque on rotor	pN-nm	–	–
τ_{reaction}	Reaction torque on stator	pN-nm	–	–
ϕ_S	Stator angular position	rad	–	–
θ_R	Rotor angular position	rad	–	–
θ_L	Load angular position	rad	–	–

RESULTS

Motor speed at low loads increases with number of stators

From simulations, we predict that the maximum speed of the motor is dependent on the number of engaged torque generating complexes (Fig. 4 *c*, *open red markers*). In their recent paper, Lo et al. computed torque-speed curves for a chimeric sodium-driven motor (28). Low-load measurements on these motors were performed using a 100 nm-diameter gold bead (Fig. 4 *c*, *inset*).

This data was collected from motors with 1–5 active stators (Fig. 4 *c*, *blue markers*). The authors focused on single-stator motor dynamics, leaving open the implications of their data for how the zero-torque speed depends on stator number. The existence of multiple discrete peaks at low load strongly supports the idea that the maximum speed is dependent on the number of stators, at least in chimeric motors. We note that such peaks have not been observed in

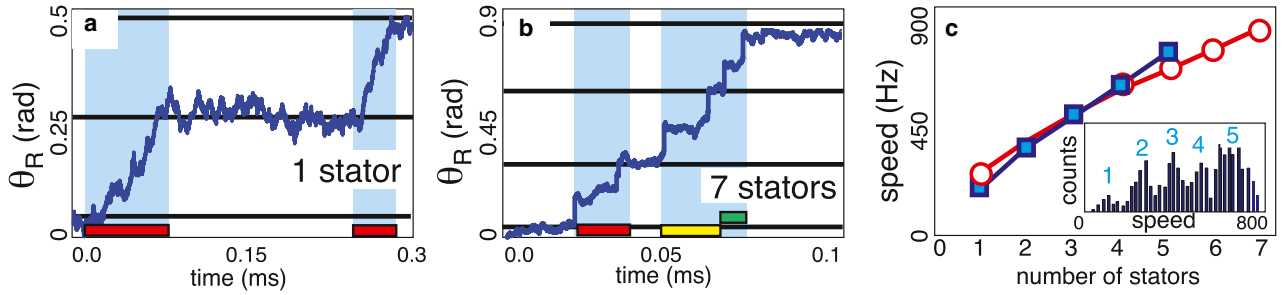

FIGURE 4 Simulated trajectories are shown for motors with (*a*) one and (*b*) seven engaged stators, with $\zeta_L = 0.005$ pN-nm-s-rad^{-1}. Horizontal black lines denote the distance between "perfect" steps ($\ell = (2\pi/26)$ rad). Colored bars at the bottom of the plots mark the duration of individual stator steps (in the shown trace, steps for three out of the seven engaged stators are shown). In the multistator motor trajectory (*b*), steps for each stator are differently colored. In accordance with published temporal resolutions (47,48), we consider two steps distinguishable if the end of the first step and the start of the second step are separated by 10 μs. These are shaded in blue; for multistator motors, steps may overlap or be too close together to be observed. (*c*) Motor speed at low loads increases with the number of stators. An experimentally measured speed distribution at low loads is shown in the inset (data from (28)). Gaussian fits to the major peaks give mean speeds (*blue squares*) in good agreement with simulation predictions (*open red circles*). To see this figure in color, go online.

wild-type motors (17), which may be due to different recruitment in proton-driven and chimeric motors (e.g., wild-type motors fail to recruit multiple stator units at very low loads). Further experiments designed with all the current knowledge in mind will be needed to resolve the exciting questions that arise from these conflicts.

Ryu and coauthors reported a set of general conditions that must be met for the limiting speed to be independent of stator number (29). First, the rate at which steps are initiated must be independent of the relative position of the rotor and the stator. This position is dependent on both the external load and the actions of any other engaged stators. Therefore, the "decision" of a stator to step should be ignorant of both these factors. Second, stators must engage the rotor for the majority of their cycle (i.e., the BFM's duty ratio $DR \approx 1$). Resurrection experiments reporting that the speed at low loads was independent of stator number soon followed (17), which seemed to lend strong support to both of the proposed requirements. We note that, although the experiments in (17) were performed in what we have considered to be near-zero load, the measurements performed in (29) that were referred to as "low load" were actually made at significantly higher loads.

Because we assume that stators are disengaged with (i.e., not applying any directional torque to) the rotor between successive power strokes, our model contains a violation of the second condition. In particular, unlike most proposed mechanisms (but see (30)), we assume motor rotation and ion flow can be loosely coupled: an ion passage may not always result in appreciable rotation of the rotor. The stator's motion, however, is tightly coupled to ion flow—that is, an ion passage is both necessary and sufficient for the initiation of a stator's power stroke. Therefore, loose coupling in our model does not arise from some form of ion leakage (30–34), but because stator steps are rarely "perfect" in multiple-stator motors. If steps overlap, a portion of the second stroke is "wasted" because the rotor is pushed out of the later-firing stator's reach.

These properties seem contrary to current assumptions that stators in the BFM must have a high duty ratio. However, we show that our prediction that $DR < 1$ at low loads arises from fundamental differences in motor dynamics between the high- and low-load regimes. In this way, we argue that our proposed mechanism is compatible with experimental evidence for a high duty ratio at high loads (Fig. 5 *a*).

Kinetically limited stators have low duty ratios

A stator initiates a step when protons arrive at a specified binding site within the complex. The mechanochemical cycle of the stator has two phases: moving and waiting, characterized by timescales T_m and T_w, respectively (18). If T_S is the time that a stator engages the rotor during a complete cycle $(T_m + T_w)$, a single-stator motor has duty ratio $DR = T_S/(T_m + T_w)$.

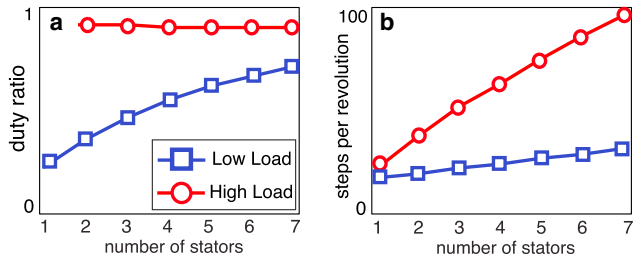

FIGURE 5 Comparison of motor dynamics at low ($\zeta_L = 0.005$ pN-nm-s-rad^{-1}, shown as *blue squares*) and high ($\zeta_L = 0.5$ pN-nm-s-rad^{-1}, shown as *red circles*) loads. (*a*) Decrease in the average time between steps with increasing stator number results in an increase in duty ratio in the low-load regime. In contrast, at high loads, each stator step takes a considerable amount of time (T_m is high), and the duty ratio is high even for single-stator motors. (*b*) As stators are recruited to fast-rotating motors (i.e., at low load), the number of independent stator steps per motor revolution (n_{steps}) increases sublinearly from 26 steps/revolution for single-stator motors. At high loads, as predicted in (37), the steps per revolution is proportional to the number of stators. Note that n_{steps} is the number of *independent* stepping events, and does not depend on experimental resolution. To see this figure in color, go online.

The waiting time between strokes T_w depends on the rate of proton arrivals at a binding site. These arrivals are Poissonian with rate $k_{on} = k_0 \exp[\lambda \Delta G_{ij}/k_B T]$. Here, ΔG_{ij} is the thermodynamic contribution of the ion motive force and $k_B T$ is Boltzmann's constant multiplied by temperature (19,35). For simplicity, we choose $\lambda = 0.5$ as done in previous studies (35). The parameter k_0 is a function of the pH of the external periplasm; lower pH corresponds to higher proton concentration and thus a speedier arrival at the site. At room temperature and pH 7.0, $\langle T_w \rangle = 1/k_{on} = 0.2$ ms for single-stator motors (18,20).

The average moving time is estimated through the relation $\omega \approx \ell/(\langle T_m \rangle + \langle T_w \rangle)$ (18). The average motor speed ω is also related to the load drag coefficient ζ_L by $\zeta_L \omega \approx \tau$, where τ is the motor torque (1,36). In our simulations, the motor is limited by proton arrivals at very low loads ($\langle T_m \rangle \approx 0.01$ ms), whereas at high loads, $\langle T_m \rangle \approx 10$ ms surpasses $\langle T_w \rangle$. These values are consistent with previous studies (18,20).

Because we predict that motor rotation is driven by steric forces, a stator must be in contact with the rotor for a large part of a productive power stroke ($T_S/T_m \approx 1$). Previous models of torque-generation have similarly considered the mechanochemical cycle of the BFM to consist of moving and waiting phases (18,20). However, our model is unique in assuming that stators disengage from the rotor between subsequent power strokes. This results in $DR < 1$ for single-stator motors at low loads, as the waiting time is no longer negligible compared with the moving time in this regime (Fig. 5 *a*, *blue squares*). The waiting time may even surpass $\langle T_m \rangle$, as shown in Fig. 4, *a* and *b*.

The waiting time until a proton binds to any one of N independently stepping stators is exponentially distributed with rate $N \times k_{on}$. Therefore, $\langle T_w \rangle$ is shortened as additional stators are recruited. The subsequent increase in duty ratio (Fig. 5 *a*, *blue squares*) results in an increase in limiting speed with the number of stators.

High duty ratios at high loads

Here, we address the assertion that the duty ratio of the BFM must be very high. Two common arguments in the literature are based on 1) the observation that the number of steps per revolution n_{steps} increases as additional torque-generating complexes were recruited (37,38), and 2) a calculation determining that a motor with a low duty ratio cannot be processive due to "unwinding" of the tether connection between the rotor and load (1). The application of these arguments, based on high-load measurements, to the low-load regime has been possible because of the lack of a proposed physical mechanism for BFM rotation. Such a mechanism is now provided in our model (21). To this end, we show these arguments can be consolidated with our proposed mechanism, as well as with the prediction that $DR < 1$ at low loads.

Samuel and Berg used fluctuation analysis to determine that the number of steps per revolution was proportional to stator number (37,38). In the absence of a specific physical mechanism, this result was interpreted to mean that a motor decreases its elementary step size as it recruits stators. This in turn implied a motor with a high duty ratio, in which each stator acts with the $N-1$ others to rotate a fixed distance d (29).

In our model, this holds in the high-load regime, where these measurements were made. Though stators disengage between strokes, the duty ratio of the motor is very high because the time spent within a power stroke is far greater than the pauses between subsequent strokes ($DR = T_s/(T_m + T_w) \approx T_s/T_m \approx 1$) (Fig. 5 *b*, *red circles*). Furthermore, the rotor is likely always in contact with at least one stator as the steps of individual stators almost certainly overlap. This accounts for the observed proportional increase in n_{steps} with the number of active stators (Fig. 5 *b*, *red circles*).

Note that stator steps still may overlap at low loads (high speeds), though they are less likely to do so because T_m is shorter than at high loads. Our simulations predict that similar analyses in this regime will detect a sublinear increase in n_{steps} with stator number (Fig. 5 *b*, *blue squares*).

The second argument was posed by Berg, who posited that if the BFM did not have a duty ratio of close to unity, it could not be processive (1). The reasoning behind this is as follows. Consider an experiment where a cell is tethered to a surface by the hook of its flagella and is spun about by the rotation of the motor at its base. The cell body is large in comparison with the flagellar motor, and accordingly the viscous drag on it is much larger than that on the BFM's rotor. Therefore, if there are no stators to prevent it, the wound tether between the surface and the cell will unwind exponentially: $\theta = \theta_0 \exp(-\alpha t)$, where θ_0 is the initial twist and α is the torsional spring constant divided by the rotational drag coefficient of the rotor. A simple calculation showed that unless a motor had a duty ratio of very close to unity, this tether would unwind too quickly for the stator units to keep up.

We note that concrete evidence is still lacking that slowly rotating tethered motors do not "lose" steps to the tether connection unwinding. Support for tightly coupled mechanisms came from reports that the number of ions per revolution was directly proportional to motor speed (39). However, it was later shown that a loosely coupled mechanism also produced a linear relationship with the same slope, but nonzero intercept (34). Regardless, our model construction and parameter choice is such that the unwinding of the tether does not overwhelm the stator in our simulations (see Supporting Material) (21). A final resolution may be reached using experiments that measure how the ion flux at stall (zero speed) differs between single- and multistator motors.

At low loads, however, the relative drags of the bead and the rotor are comparable. As we approach the zero-torque limit, the rotor drag may surpass that of the load (18,20). For example, we estimated the drag coefficient for the low-load measurement in (28) to be $\zeta_L \approx 0.005$ pN-nm-s-rad^{-1}, which is lower than $\zeta_R \approx 0.02$ pN-nm-s-rad^{-1} (1). In this case, the bead will move forward as the tether connection unwinds.

More generally, the characteristic timescale of the load's motion is given by its frictional drag coefficient divided by the spring constant: $t_L = \zeta_L/\kappa$. A single-stator motor should have a comparably long power stroke. Note that this is not necessary for a multistator motor: steps from different stators may overlap, extending the period during which at least one complex is present.

To illustrate, we consider the second-smallest bead used by Lo et al. (28). Estimating $\zeta_L = 0.04$ pN-nm-s-rad^{-1} and choosing a spring constant $\kappa = 150$ pN-nm-rad^{-1} at the lower edge of the measured range (40), the characteristic timescale of the load is $t_L = \zeta_L/\kappa \approx 0.27$ ms. A single-stator motor with this load rotated at ≈ 110 Hz (28). Recall that motor speed $\omega \approx \ell/(\langle T_m \rangle + \langle T_w \rangle)$, where the step size $\ell = (1/26)$ revolution and $\langle T_w \rangle \approx 0.2$ ms. Then $\langle T_m \rangle \approx (1/26)/110 - 2$ e-4 ≈ 0.15 ms, and the load is able to (at least partially) catch up to the rotor.

DISCUSSION

The dynamics of the BFM across applied loads have been of great interest since a two-regime torque-speed curve was proposed several decades ago. Recent experiments reporting that the number of stators in a motor varies across loads have opened some interesting questions, and reopened several more.

For instance, the zero-torque speed has been assumed to be independent of the number of docked stators based on the results of early resurrection experiments (15–17). Theoretical models after these results were reported have all been constructed to reproduce this behavior at low loads. However, recent experiments strongly suggest that these experiments were never performed on motors with more than a single stator (13), making revisiting this long-held assumption timely.

We note that ~25% of the zero-load motors measured in (13) were interpreted to have two, instead of one, stators. However, it was noted by the authors that motors that were interpreted to have two stators likely had flagella that were incompletely sheared, which may have resulted in an increased load for these motors. Furthermore, this result was reached using a relatively small number of data points, making a statistically significant conclusion difficult to reach. The idea that the stator number varies with load is quite new, and further experiments on the low-load behavior of this motor performed with this knowledge are needed for conclusive evidence in any direction.

In opposition to current assumptions, our simulations predict that the zero-torque speed of the BFM increases with stator number. We note that there was an earlier model that predicted that the motor's speed at low load was not universal (35). However, the mechanism suggested in (35) was a tightly coupled one that predicted that this speed would *decrease* with an increasing number of stators. Experiments by Lo et al. (28) (shown in Fig. 4 *c*) seem to support the opposite trend in chimeric motors, as predicted by our model. However, as such peaks have not been observed in wild-type motors, further experiments at low load are required to make any definitive conclusions. As we mentioned previously, tightly coupled mechanisms can be differentiated from ours by an experiment testing the intercept of the relationship between the number of ions per revolution and motor speed (34).

Our prediction arises from our assumption that stators detach from the motor when they pause between steps. This assumption is common to most models in which a conformational change in the stator drives motor rotation. This results in a low duty ratio for motors at low load, where the waiting time between steps is at least on the order of the time spent in a power stroke. Because the power stroke duration is much longer at high loads, the duty ratio in this regime is not affected by this unbound state. In this way, our mechanism is consistent with evidence that processive motors at high load must have a high duty ratio.

It is important to note that we do not propose that there exists *no* top speed to the motor at low loads: the moving time T_m at zero-torque still takes some, albeit not much, time. The limiting speed of the motor at low loads will occur when the duty ratio of the motor approaches 1 (i.e., when the waiting time between subsequent power strokes T_w no longer significantly decreases with the recruitment of additional stators). Our simulations suggest, however, that this top speed might not be reached by motors with close to the maximum number of observed stators (Fig. 4 *c*), let alone by single-stator motors.

Recently, Lo et al. presented evidence of increasing zero-torque speed with stator number in chimeric, sodium-driven motors (28). However, this result was not fully explored as the authors focused on understanding single-stator motor dynamics. Further experiments, especially on wild-type motors, would directly test the hypothesis presented here. Although previous experiments have clarified other aspects of low-load motor behavior (41–43), the explicit characterization of the dependence of the limiting speed on the number of stator units deserves a more-focused study.

The discovery that stator recruitment in the flagellar motor is dynamic and load-dependent forces us to go back and reconsider many things that were considered common knowledge in the field. We certainly do not claim that the current published data on the wild-type H^+ motor support or validate our model (though there is support in the sodium-driven motor). However, in light of the evidence found

in this study, we do claim that further experiments are required to reach any definitive conclusions.

We hope this work has emphasized that even questions long believed to be closed must be periodically critically examined when new information arises. We strongly hope that our proposal of this model will reinvigorate the question of how the flagellar motor's low-load speed depends on stator number, and, in particular, will provide the momentum for experiments conducted with all the current knowledge taken into account.

SUPPORTING MATERIAL

Supporting discussion and three figures are available at http://www.biophysj.org/biophysj/supplemental/S0006-3495(16)30518-5.

AUTHOR CONTRIBUTIONS

J.A.N., R.M.B., and G.O. designed research; J.A.N. performed research and analyzed data; J.A.N., R.M.B, and G.O. wrote the article.

ACKNOWLEDGMENTS

The authors thank Ashley Nord for many helpful discussions.

Funding was provided by NIH grant R01- GM110066 (to G.O. and J.A.N) and an NSF IGERT administered by the Center for Integrative Biomechanics in Education and Research (to J.A.N.). R.M.B. was supported by the Biotechnology and Biological Sciences Research Council and the Engineering and Physical Sciences Research Council.

REFERENCES

1. Berg, H. C. 2003. The rotary motor of bacterial flagella. *Annu. Rev. Biochem.* 72:19–54.
2. Korobkova, E. A., T. Emonet, …, P. Cluzel. 2006. Hidden stochastic nature of a single bacterial motor. *Phys. Rev. Lett.* 96:058105.
3. Bai, F., R. W. Branch, …, R. M. Berry. 2010. Conformational spread as a mechanism for cooperativity in the bacterial flagellar switch. *Science.* 327:685–689.
4. Sourjik, V., and N. S. Wingreen. 2012. Responding to chemical gradients: bacterial chemotaxis. *Curr. Opin. Cell Biol.* 24:262–268.
5. Lloyd, S. A., F. G. Whitby, …, C. P. Hill. 1999. Structure of the C-terminal domain of FliG, a component of the rotor in the bacterial flagellar motor. *Nature.* 400:472–475.
6. Brown, P. N., C. P. Hill, and D. F. Blair. 2002. Crystal structure of the middle and C-terminal domains of the flagellar rotor protein FliG. *EMBO J.* 21:3225–3234.
7. Lee, L. K., M. A. Ginsburg, …, D. Stock. 2010. Structure of the torque ring of the flagellar motor and the molecular basis for rotational switching. *Nature.* 466:996–1000.
8. Zhou, J., S. A. Lloyd, and D. F. Blair. 1998. Electrostatic interactions between rotor and stator in the bacterial flagellar motor. *Proc. Natl. Acad. Sci. USA.* 95:6436–6441.
9. Braun, T. F., L. Q. Al-Mawsawi, …, D. F. Blair. 2004. Arrangement of core membrane segments in the MotA/MotB proton-channel complex of *Escherichia coli*. *Biochemistry.* 43:35–45.
10. Lowder, B. J., M. D. Duyvesteyn, and D. F. Blair. 2005. FliG subunit arrangement in the flagellar rotor probed by targeted cross-linking. *J. Bacteriol.* 187:5640–5647.
11. Khan, I. H., T. S. Reese, and S. Khan. 1992. The cytoplasmic component of the bacterial flagellar motor. *Proc. Natl. Acad. Sci. USA.* 89:5956–5960.
12. Suzuki, H., K. Yonekura, and K. Namba. 2004. Structure of the rotor of the bacterial flagellar motor revealed by electron cryomicroscopy and single-particle image analysis. *J. Mol. Biol.* 337:105–113.
13. Lele, P. P., B. G. Hosu, and H. C. Berg. 2013. Dynamics of mechanosensing in the bacterial flagellar motor. *Proc. Natl. Acad. Sci. USA.* 110:11839–11844.
14. Tipping, M. J., N. J. Delalez, …, J. P. Armitage. 2013. Load-dependent assembly of the bacterial flagellar motor. *MBio.* 4, e00551-e13.
15. Block, S. M., and H. C. Berg. 1984. Successive incorporation of force-generating units in the bacterial rotary motor. *Nature.* 309:470–472.
16. Reid, S. W., M. C. Leake, …, R. M. Berry. 2006. The maximum number of torque-generating units in the flagellar motor of *Escherichia coli* is at least 11. *Proc. Natl. Acad. Sci. USA.* 103:8066–8071.
17. Yuan, J., and H. C. Berg. 2008. Resurrection of the flagellar rotary motor near zero load. *Proc. Natl. Acad. Sci. USA.* 105:1182–1185.
18. Meacci, G., and Y. Tu. 2009. Dynamics of the bacterial flagellar motor with multiple stators. *Proc. Natl. Acad. Sci. USA.* 106:3746–3751.
19. Bai, F., C.-J. Lo, …, J. Xing. 2009. Model studies of the dynamics of bacterial flagellar motors. *Biophys. J.* 96:3154–3167.
20. Meacci, G., G. Lan, and Y. Tu. 2011. Dynamics of the bacterial flagellar motor: the effects of stator compliance, back steps, temperature, and rotational asymmetry. *Biophys. J.* 100:1986–1995.
21. Mandadapu, K. K., J. A. Nirody, …, G. Oster. 2015. Mechanics of torque generation in the bacterial flagellar motor. *Proc. Natl. Acad. Sci. USA.* 112:E4381–E4389.
22. Kojima, S., and D. F. Blair. 2001. Conformational change in the stator of the bacterial flagellar motor. *Biochemistry.* 40:13041–13050.
23. Nishihara, Y., and A. Kitao. 2015. Gate-controlled proton diffusion and protonation-induced ratchet motion in the stator of the bacterial flagellar motor. *Proc. Natl. Acad. Sci. USA.* 112:7737–7742.
24. Sowa, Y., A. D. Rowe, …, R. M. Berry. 2005. Direct observation of steps in rotation of the bacterial flagellar motor. *Nature.* 437:916–919.
25. Paul, K., G. Gonzalez-Bonet, …, D. Blair. 2011. Architecture of the flagellar rotor. *EMBO J.* 30:2962–2971.
26. Barcilon, V. 1992. Ion flow through narrow membrane channels: Part I. *SIAM J. Appl. Math.* 52:1391–1404.
27. Luchinsky, D., R. Tindjong, …, R. Eisenberg. 2008. Ion channels as electrostatic amplifiers of charge fluctuations. *In* Journal of Physics: Conference Series, *Vol. 142*. IOP Publishing, Bristol, UK, p. 012049.
28. Lo, C.-J., Y. Sowa, …, R. M. Berry. 2013. Mechanism and kinetics of a sodium-driven bacterial flagellar motor. *Proc. Natl. Acad. Sci. USA.* 110:E2544–E2551.
29. Ryu, W. S., R. M. Berry, and H. C. Berg. 2000. Torque-generating units of the flagellar motor of *Escherichia coli* have a high duty ratio. *Nature.* 403:444–447.
30. Boschert, R., F. R. Adler, and D. F. Blair. 2015. Loose coupling in the bacterial flagellar motor. *Proc. Natl. Acad. Sci. USA.* 112:4755–4760.
31. Oosawa, F., and J. Masai. 1982. Mechanism of flagellar motor rotation in bacteria. *J. Phys. Soc. Jpn.* 51:631–641.
32. Oosawa, F., and S. Hayashi. 1983. Coupling between flagellar motor rotation and proton flux in bacteria. *J. Phys. Soc. Jpn.* 52:4019–4028.
33. Oosawa, F., and S. Hayashi. 1986. The loose coupling mechanism in molecular machines of living cells. *Adv. Biophys.* 22:151–183.
34. Berry, R. M. 1993. Torque and switching in the bacterial flagellar motor. An electrostatic model. *Biophys. J.* 64:961–973.
35. Xing, J., F. Bai, …, G. Oster. 2006. Torque-speed relationship of the bacterial flagellar motor. *Proc. Natl. Acad. Sci. USA.* 103:1260–1265.
36. Inoue, Y., C.-J. Lo, …, A. Ishijima. 2008. Torque-speed relationships of Na+-driven chimeric flagellar motors in *Escherichia coli*. *J. Mol. Biol.* 376:1251–1259.

37. Samuel, A. D., and H. C. Berg. 1995. Fluctuation analysis of rotational speeds of the bacterial flagellar motor. *Proc. Natl. Acad. Sci. USA.* 92:3502–3506.

38. Samuel, A. D., and H. C. Berg. 1996. Torque-generating units of the bacterial flagellar motor step independently. *Biophys. J.* 71:918–923.

39. Meister, M., and H. C. Berg. 1987. The stall torque of the bacterial flagellar motor. *Biophys. J.* 52:413–419.

40. Block, S. M., D. F. Blair, and H. C. Berg. 1989. Compliance of bacterial flagella measured with optical tweezers. *Nature.* 338:514–518.

41. Yuan, J., K. A. Fahrner, and H. C. Berg. 2009. Switching of the bacterial flagellar motor near zero load. *J. Mol. Biol.* 390:394–400.

42. Yuan, J., and H. C. Berg. 2010. Thermal and solvent-isotope effects on the flagellar rotary motor near zero load. *Biophys. J.* 98:2121–2126.

43. Wang, F., J. Yuan, and H. C. Berg. 2014. Switching dynamics of the bacterial flagellar motor near zero load. *Proc. Natl. Acad. Sci. USA.* 111:15752–15755.

44. Zhou, J., R. T. Fazzio, and D. F. Blair. 1995. Membrane topology of the MotA protein of *Escherichia coli*. *J. Mol. Biol.* 251:237–242.

45. Yuan, J., K. A. Fahrner, …, H. C. Berg. 2010. Asymmetry in the clockwise and counterclockwise rotation of the bacterial flagellar motor. *Proc. Natl. Acad. Sci. USA.* 107:12846–12849.

46. Chen, X., and H. C. Berg. 2000. Torque-speed relationship of the flagellar rotary motor of *Escherichia coli*. *Biophys. J.* 78:1036–1041.

47. Nishiyama, M., H. Higuchi, and T. Yanagida. 2002. Chemomechanical coupling of the forward and backward steps of single kinesin molecules. *Nat. Cell Biol.* 4:790–797.

48. Kolomeisky, A. B., and M. E. Fisher. 2007. Molecular motors: a theorist's perspective. *Annu. Rev. Phys. Chem.* 58:675–695.

Biophysical Journal, Volume *111*

Supplemental Information

The Limiting Speed of the Bacterial Flagellar Motor

Jasmine A. Nirody, Richard M. Berry, and George Oster

Supplementary Material for

The Limiting Speed of the Bacterial Flagellar Motor

J.A. Nirody, R.M. Berry, G. Oster†

Contents

1 Model for torque generation in the BFM

In this section, we provide Langevin equations describing the dynamics of the stator, the rotor, and the load. A more detailed description of the model can be found in [1]. We also detail how the single-stator model can be extended to deal with motors with multiple stators. All simulation code will be made available at http://www.ocf.berkeley.edu/∼jnirody.

Stators have four "loops" which dip into the cytoplasm and can generate torque by pushing on the "spokes" of the rotor. In our model, two loops are involved in torque-generation in the counterclockwise direction, while the other two generate clockwise movement. The numbering of these loops is arbitrary. Prior to the start of the cycle, we assume that electrostatic interactions between charged residues on the stator and rotor place them within close proximity of each other.

1.1 Single-stator equations

This model was originally presented and described in detail for single-stator motors in our previous work [1]. We review some important details in this section. The dynamics of the stator, rotor, and load are described by the following Langevin equations:

$$\textbf{Stator :} \qquad \zeta_S \frac{d\phi_S}{dt} = \underbrace{F_p \ell_p}_{\substack{\text{Torque from} \\ \text{Proline hinge}}} - \underbrace{\tau_{\text{reaction}}}_{\substack{\text{Reaction} \\ \text{from rotor}}} + \underbrace{\sqrt{2k_BT\zeta_S} f_n(t)}_{\text{Thermal fluctuations}} \tag{1}$$

$$\textbf{Rotor :} \qquad \zeta_R \frac{d\theta_R}{dt} = \underbrace{\tau_{\text{contact}}}_{\substack{\text{Torque} \\ \text{from stator}}} - \underbrace{\kappa(\theta_R - \theta_L)}_{\substack{\text{Spring connection} \\ \text{to load}}} + \underbrace{\sqrt{2k_BT\zeta_R} f_n(t)}_{\text{Thermal fluctuations}} \tag{2}$$

$$\textbf{Load :} \qquad \zeta_L \frac{d\theta_L}{dt} = \underbrace{\kappa(\theta_R - \theta_L)}_{\substack{\text{Spring connection} \\ \text{to rotor}}} + \underbrace{\sqrt{2k_BT\zeta_L} f_n(t).}_{\text{Thermal fluctuations}} \tag{3}$$

Here ζ_S, ζ_R, and ζ_L are the effective drag coefficients of the stator, rotor, and load. The last term in each equation is the stochastic Brownian force, where $f_n(t)$ is uncorrelated white noise.

In Equation (1), the internal torque driving the stator due to the rearrangement of hydrogen bonds caused by a proton binding event is denoted by $F_p\ell_p$. Because the motion of the two halves of the power stroke are mechanically equivalent, we collapse the dynamics of the two loops into a single equation.

The stator free energy potential $G = G(\phi_S, j)$ is shown in the right panel of Figure S1. Before the cations bind to the stator, the motion of the stators is governed by the potential $G_1(\phi_S)$ where the minimum is around $\phi_S = 0°$ as shown in the right panel of Figure S1. After the cations bind, the stator potential switches from G_1 to G_2. This compels the stator angle to move from $\phi_S = 0°$ to $\phi_S = 20°$. During this transformation, the loop pushes the rotor via a steric force. At the end of the conformational change, when the loops are at the minimum of the potential G_2, the cations exit into the cytoplasm. The potential then switches back to G_1 and the loops traverse back to $\phi_S = 0°$. During this time, the loops apply a contact force on the same rotor spoke as in the previous substep.

For ease of computation, we approximate the potential using a piecewise function:

$$G_1(\phi) = \begin{cases} \beta\ell_p\phi^2 & \text{if } \phi \le 0 \\ F_p\ell_p\phi & \text{if } 0 \le \phi \le \phi_{max} \\ F_p\ell_p\phi_{max} + \beta\ell_p(\phi - \phi_{max})^2 & \text{if } \phi \ge \phi_{max} \end{cases}$$

and

$$G_2(\phi) = \begin{cases} \beta\ell_p\phi^2 & \text{if } \phi \le 0 \\ -F_p\ell_p\phi & \text{if } 0 \le \phi \le \phi_{max} \\ -F_p\ell_p\phi_{max} + \beta\ell_p(\phi - \phi_{max})^2 & \text{if } \phi \ge \phi_{max}. \end{cases}$$

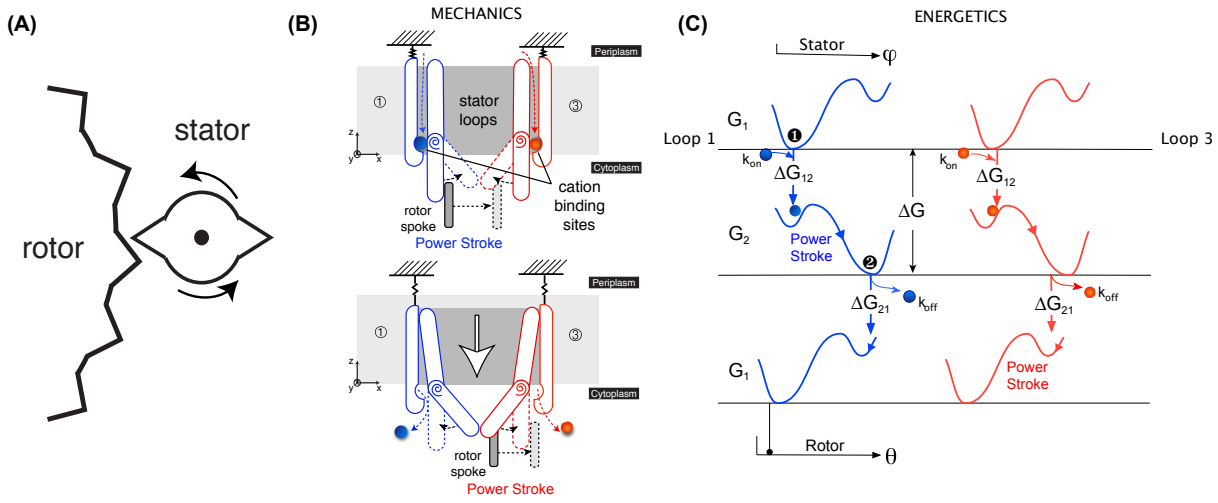

Figure S1: Dynamics of the rotor-stator interaction. **(a)** A generalized version of the mechanism from [1]. The stator can be considered a gear with two spokes. Each stator spoke is in contact with a spoke on the rotor for a small portion of a "revolution" of the stator gear. The spacing of the stator spokes depends on the relative values of k_{on} and k_{off}. The figure shows an example where the on and off rates are equal, and so the spokes are evenly spaced around the periphery of the gear. In this context, the dependence of the zero-torque speed on the number of stators can be explained easily as follows: since each stator applies force for a short duration of time. Because the impulses from different stators rarely overlap, their effects are additive. **(b)** MECHANICS OF THE POWER STROKE. *Top panel:* Cation binding induces a strain in the stator, which causes the loops to bend. This results in the first half of the power stroke (here, by Loop 1), and sets up the second loop (here, Loop 3) to perform its half of the power stroke. Subsequently, the cations are released into the cytoplasm. This occurs because our proposed motion also has a vertical component—the loops lower themselves out of the membrane. This release then reverses the strain and causes the loops to restraighten. This results in the second half of the power stroke. We note that this image depicts a two-dimensional projection of a three-dimensional motion: the motion of the stators is not constrained to the plane of the page. **(c)** ENERGETICS OF THE POWER STROKE. Because the two loops move in-phase with each other in our model, their energetic pictures are identical. We describe the free energy landscapes using double-well Landau potentials (G_1 for the first half of the power stroke, and G_2 for the second half). These landscapes are shown in blue for Loop 1 and red for Loop 3 with respect to the angles of the stator ϕ and rotor θ. The initial entrance of the proton into the ion channel (k_{on}) places the system within k_BT of the energy barrier. Thermal motions then result in the first half of the power stroke. The exit of the protons into the cytoplasm (k_{off}) results in the "reset", and the second half of the power stroke. Figure modified from [1].

The transition rates between the two potentials are given by the rates of protons "hopping on" and "hopping off" of the stator binding sites. To satisfy detailed balance when the ion-motive force (IMF) is non-zero, the kinetic coefficients for the reaction are chosen so that

$$\frac{k_{\text{on}}}{k_{\text{off}}} = 10^{(\text{pK}_\text{a}^p - \text{pH}_\text{periplasm})} \exp\left(\frac{\Delta G_{ij}}{k_B T}\right), \tag{4}$$

where ΔG_{ij} is the thermodynamic contribution of the IMF (see Figure S1) and $k_B T$ is Boltzmann's constant multiplying temperature. Since G_1 and G_2 are simply horizontal reflections of one another, $\Delta G_{12} = \Delta G_{21}$. For convenience, we choose the following with $\lambda = 0.5$:

$$k_{\text{on}} = 10^{-\text{pH}_\text{periplasm}} \exp\left(\lambda\Big(\frac{\Delta G_{ij}}{k_B T}\Big)\right), \tag{5}$$

$$k_{\text{off}} = 10^{-\text{pK}_\text{a}^p} \exp\left(-(1-\lambda)\Big(\frac{\Delta G_{ij}}{k_B T}\Big)\right). \tag{6}$$

The contact torque applied to the rotor (in Equation (2)), and consequent reaction torque applied to the stator (in Equation (1)), are given by τ_{contact} and τ_{reaction} respectively. The values for these torques are calculated by taking the gradient of the interaction potential between the rotor and stator; in particular: the torque on the rotor can be obtained as $\tau_{\text{contact}} = -\frac{\partial V_{RS}}{\partial \theta_R}$ and the reaction torque on the stator is $\tau_{\text{reaction}} = -\frac{\partial V_{RS}}{\partial \phi_S}$.

The steric interaction potential is simulated using a soft linear repulsive force with a cutoff distance X_{RS}:

$$V_{RS}(\phi_S^i, \theta_R) = \begin{cases} -F_{RS}\frac{(R\theta_R - \ell_P\phi_S)^2}{X_{RS}} & \text{if } 0 \le x \le X_{RS} \\ 0 & \text{otherwise,} \end{cases}$$

Therefore, $\tau_{\text{contact}} = -\frac{\partial V_{RS}}{\partial \theta_R}$ is given by:

$$\tau_{\text{contact}}(x) = \begin{cases} -2F_{RS}R\frac{R\theta_R - \ell_P\phi_S}{X_{RS}} = 2F_{RS}R\left(1 - \frac{x_{RS}}{X_{RS}}\right) & \text{if } 0 \le x_{RS} \le X_{RS} \\ 0 & \text{otherwise,} \end{cases}$$

and τ_{reaction} by:

$$\tau_{\text{reaction}}(x) = \begin{cases} 2F_{RS}\ell_P\frac{R\theta_R - \ell_P\phi_S}{X_{RS}} = -2F_{RS}\ell_P\left(1 - \frac{x_{RS}}{X_{RS}}\right) & \text{if } 0 \le x_{RS} \le X_{RS} \\ 0 & \text{otherwise,} \end{cases}$$

Here, F_{RS} is the maximum force that can be applied by the proline hinge and $x_{RS} = X_{RS} + R\theta_R - \ell_p\phi_S$ denotes the distance between the position of the stator loop and the nearest FliG. We choose $F_{RS} = F_p$. All other parameters are defined as described in the main text.

The rotor and load are connected by a linear spring with constant κ; the elastic coupling terms in the equations for the rotor and the load thus appear with opposite signs (in Equations (2) and (3), respectively). The elastic constant in the experiments can vary depending on the length of the hook when attaching the bead. In some cases, the hook is cut very short or is stiffened by an antibody linker, which would correspond to a large spring coefficient [2].

Single-stator trajectories at varying loads are shown in Figure S2. It is apparent from these that increasing the load increases the time stators spend within a power stroke (T_m), and thus reduces the proportion of the time the stator is disengaged from the rotor (i.e., higher loads increase the duty ratio).

Another logical consideration for experimentally testing this model with respect to the duty ratio is to target the parameters which are affected by the IMF. Raising the IMF will increase the rate of proton arrivals at the stator, lowering T_w; however the IMF may also have an effect on the energy available to the stator during a power stroke, thus increasing the force it can apply to the rotor. This, in turn, may speed up the power stroke, lowering T_m as well, making it difficult to predict within the context of our current model how these two factors would balance our and effect the duty ratio of the motor.

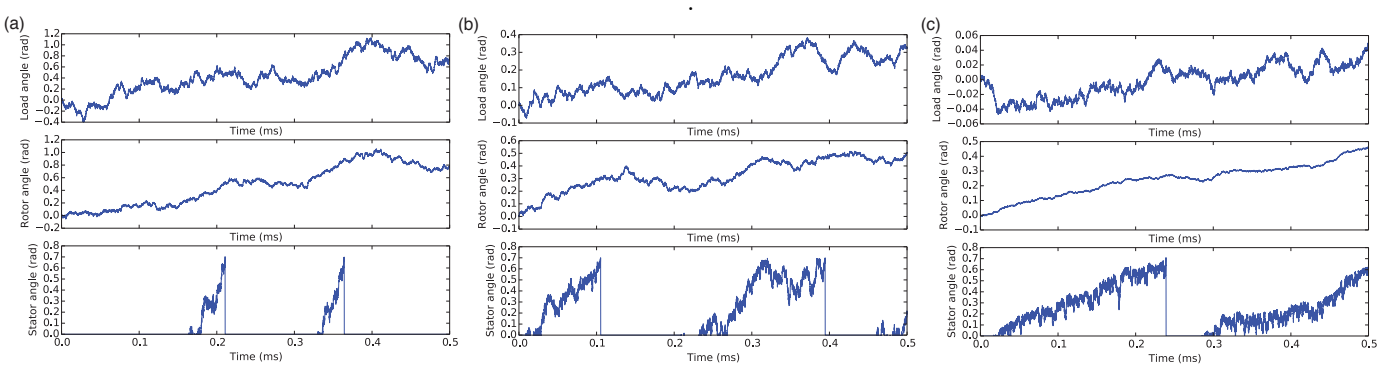

Figure S2: Simulation output (0.5 ms) for a single-stator motor at **(a)** $\zeta_L = 0.005$ pN-nm-s-rad^{-1}, **(b)** $\zeta_L = 0.05$ pN-nm-s-rad^{-1}, and **(c)** $\zeta_L = 0.5$ pN-nm-s-rad^{-1}. The duration of stator steps (bottom panel) increases with load, decreasing the relative amount of a mechanochemical cycle taken up by the waiting time between subsequent steps.

1.2 Extension to multiple-stator motors

In a motor with multiple stators, the mechanics of each stator are as described above. The mechanics of each unit follows the equations presented for a single stator. In particular, each stator is independently "activated" at rates given by Equations (5) and (6). Because cation arrivals are Poisson processes (i.e., waiting times between arrivals are distributed exponentially) [3, 4], the "next arrival" in a motor with N stators occurs at a rate $N \times k_{\text{on}}$, where k_{on} is the rate of arrival for a single stator.

This is seen in Figure S3, where the space between individual stator stepping events is much smaller in a motor with seven stators (right) than in a single-stator motor (left). The decrease in waiting time between steps in multi-stator motors is also seen in the rotor and bead trajectories, which are far smoother when steps follow each other more closely.

In a multi-stator motor, the total contact torque τ_{contact} that the rotor feels is given by a sum of the contributing contact torques of each stator at a given time:

$$\tau_{\text{contact}} = \sum_{i=1}^{N} \tau^i_{\text{contact}}, \tag{7}$$

where τ^i_{contact} corresponds to the contribution of the ith stator and N is the total number of docked stators in the motor. The reaction torque, τ_{reaction} is computed accordingly. As is evident from the form of the stator-rotor interaction potential V_{RS}, a stator not in a power stroke (i.e., during T_w) applies no torque to the rotor (i.e., $\tau^i_{\text{contact}} = \tau^i_{\text{reaction}} = 0$).

Let us consider duty ratio as the proportion of time that the torque on the rotor from the stator is nonnegligible. Then, from the above, it is clear that, by the construction of our model, more docked stators increase a motor's duty ratio: a multi-stator motor, with many possibly contributing terms to the sum would naturally have a higher duty ratio than a single stator motor.

An important consideration in simulations with multiple, independently-stepping stators is the following. While each stator pushes on its own "spoke" on the rotor's edge, these spokes are rigidly connected. This means that if one stator begins its power stroke shortly after another stator has done so, it likely will apply no torque to the rotor for some portion of its cycle. This is because the positions of the rotor spokes are dependent on each other, and the power stroke of the first stator will have pushed the second stator's spoke slightly out of reach (at least for the initial part of its cycle).

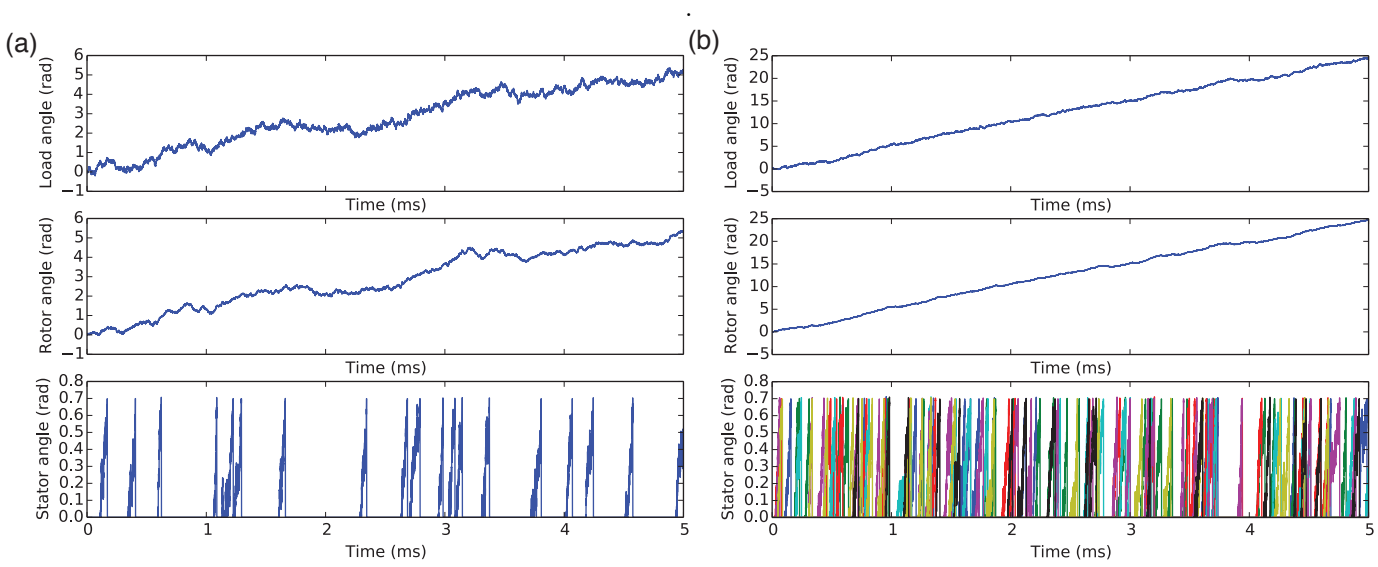

Figure S3: Simulation output (5 ms) at $\zeta_L = 0.005$ pN-nm-s-rad^{-1} for motors with **(a)** one and **(b)** seven stators. Top and middle panels show load and rotor trajectories, respectively. Bottom panels show stator stepping events. In **(b)**, events for each stator are colored uniquely.

2 Numerical implementation

In this section, we discuss briefly some technical details regarding the implementation of the above systems of equations. Simulations of Langevin dynamics were written in Python 2.7. Example low-load simulation output can be seen for motors with one and seven stators in Figure S3.

Discrete transitions are modeled using Gillespie's method, as follows. For motors with N stators, N 'first arrival times' are initially chosen from an exponential distribution at $t = 0$. Each subsequent waiting time is drawn from an exponential distribution when the stator loop reached a small range around the potential minima. For example, the time required to "hop off" is chosen when the angle of the stator loop is within a small range $(20 - \epsilon^\circ, 20 + \epsilon^\circ)$ for some prescribed ϵ. Likewise, the time for the next cation arrival is chosen when the angle retracts to within ϵ of 0°. This is done to imitate the alternating access of the cation-binding site to the periplasm and cytoplasm.

The rate for protons hopping off into the cytoplasm (k_{off}) are chosen as 1000 times the value for proton arrivals k_{on} [5]. This is in line with the fact that half-steps have yet to be directly observed experimentally.

Continuous-time portions of each cycle (corresponding to the mechanical movements) for the stator, rotor, and load are simulated using a forward finite difference scheme with a time step of 10^{-8} s. Checks are put in place to assure that the stator position does not surpass the position of the rotor due to the time step being too large.

Rotor spokes (FliG proteins) are rigidly connected to each other. Therefore, if a stator s_1 initiates its power stroke at time t_1 and a second stator s_2 initiates its power stroke at time $t_2 > t_1$, then the FliG adjacent to s_2 will have moved the same distance as the FliG that s_1 pushed in the interval $[t_1, t_2)$. This means that the portion of the power stroke up until s_2 can "catch up" to the FliG in front of it will be 'wasted' (i.e., no torque will be applied on the rotor by s_2). For simplicity, we do not consider backsteps in our simulations: each stator sees only the FliG in front of it. In time intervals where no stators are pushing on the rotor, stators are repositioned such that each is directly adjacent to a FliG.

All data points were computed as averages from 10 simulation runs, each of length 1 s. Because simulations were performed at low load, this run length was sufficient to include many steps. Standard errors of the mean were smaller than the size of markers.

3 Tether-wind calculation

In his 2003 review article, Howard Berg posed an argument for why torque-generating units in the flagellar motor must have a very high duty ratio [6]. This "tether-wind" argument is summarized in the main text. Here, we redo this calculation with the values Berg originally used, and then revise it using our model construction and chosen parameters (given in Table 1 in the main text). Though high-load simulations were not used in the conclusions for this manuscript, this section provides an explanation as to how high-load simulations were run in our previous paper [1].

Consider a cell tethered to a surface by its flagellar filament. The cell is spun around by the rotation of the motor at the base of the filament. In the first step of a resurrection experiment, a motor has a single torque-generating unit.

Berg estimated the torque generated by a wild-type motor (with 8 torque-generating units) to be 4000 pN-nm, so that each unit generates about 500 pN-nm of torque. Likewise, he estimated the torsional spring constant of the tether to be 500 pN-nm-rad^{-1}, leading to a twist in the tether of about 1 rad (57°). Since the cell body has a significantly higher drag than the rotor, the tether will unwind exponentially once the stator disengages: $\theta = \theta_0 \exp(-\alpha t)$, where θ_0 is the initial twist and α is the torsional spring constant divided by the drag coefficient of the rotor. Estimating the drag of the rotor as 0.02 pN-nm-s-rad^{-1}, $\alpha = 2.5 \times 10^{-4}$ s^{-1}. Then, if the stator is disengaged for 1.6×10^{-5} s (corresponding to a duty ratio of 0.999 in his calculation), the twist in the tether decreases to $57 \exp(-2.5 \times 10^4 \times 1.6 \times 10^{-5}) = 38°$, or by 19°. At the time of the publication, it was assumed that a single unit steps 50 times per revolution, so that a single step was approximately 7.2°, or less than half of the unwinding. This led to the conclusion that a single torque generator would not be able to keep up if it detached for a time even on the order of 10^{-5} s.

Most estimates have calculated the maximum torque in the BFM to be approximately 2000 pN-nm. Assuming a motor at stall has 11 stators, each stator generates approximately 180 pN-nm of torque. This is also consistent with single-stator measurements in chimeric motors [7]. We estimate the torsional spring constant very conservatively, at the lower end of the experimentally measured range, as 150 pN-nm-rad^{-1} [2]. Then, the tether is twisted by 1.2 rad, or 69°.

The "waiting time" between subsequent steps corresponds to the time required for an ion from the periplasm to bind to an exposed binding site on the stator. In our model simulations, this site is exposed when the angle of the stator $\phi_S < 0 + \epsilon$. Recall that $\langle T_w \rangle = 0.2$ ms. A stator disengages from the rotor from the time it completes its power stroke ($\phi_S \leq 0$) until an ion binds to it. In our simulations, when ϕ_S is in the interval $(0, 0 + \epsilon)$, it is able to bind a periplasmic cation while still being bound to the rotor. We take ϵ to be very small, $\frac{\pi}{1500}$ rad = 0.12°. For the vast majority of the loads considered, the time spent in this interval is negligible compared to $\langle T_w \rangle$, and the stator detaches from the rotor for 0.2 ms at a time, on average. However, in very slowly-rotating motors, the time when $\phi_S \in (0, 0 + \epsilon)$ may be large enough to significantly lower the average time that the stator detaches from the rotor.

Tethered cells rotated at 1.2 Hz, which corresponds to each step taking 32 ms (assuming there are 26 steps per revolution). Since the experiment is at very high load $\langle T_m \rangle \approx 32$ ms, since $\langle T_m \rangle \gg \langle T_w \rangle$. Because the BFM lives at low Reynolds number, we assume that the stator moves at a constant speed throughout its power stroke. Then $\phi_S \in (0, 0 + \epsilon)$ for $0.12°/20° = 0.006$ of $\langle T_m \rangle$, or 0.192 ms. Then, the average time that the stator is actually detached from the rotor between consecutive strokes at the load considered in our simulations is 0.008 ms. During this time, the tether unwinds to $69 \exp(-150/0.02 \times 8 \times 10^{-6}) \approx 65°$, or by 4°. This is less than our assumed elementary step length, $2\pi/26 \approx 14°$.

However, we note here once again, as in the main text, that there is not yet concrete evidence that a single-stator motor at very high load does not, in fact, "lose" several steps to the unwinding of the tether connection. This uncertainty will likely be resolved only by experiments which can quantify how the ion flux varies between single- and multi-stator motors (i.e., motors with different duty ratios) at high loads.

References

[1] K. K. Mandadapu, J. A. Nirody, R. M. Berry, and G. Oster, Proceedings of the National Academy of Sciences **112**, E4381 (2015).

[2] S. M. Block, D. F. Blair, and H. C. Berg, Nature **338**, 514 (1989).

[3] V. Barcilon, SIAM Journal on Applied Mathematics **52**, 1391 (1992).

[4] D. Luchinsky, R. Tindjong, I. Kaufman, P. McClintock, and R. Eisenberg, in *Journal of Physics: Conference Series* (IOP Publishing, 2008), vol. 142, p. 012049.

[5] U. Alexiev, R. Mollaaghababa, P. Scherrer, H. Khorana, and M. Heyn, Proceedings of the National Academy of Sciences **92**, 372 (1995).

[6] H. C. Berg, Annual Review of Biochemistry **72**, 19 (2003).

[7] C.-J. Lo, Y. Sowa, T. Pilizota, and R. M. Berry, Proceedings of the National Academy of Sciences **110**, E2544 (2013).

[8] P. P. Lele, B. G. Hosu, and H. C. Berg, Proceedings of the National Academy of Sciences **119**, 11839 (2013).

[9] J. Yuan and H. C. Berg, Proceedings of the National Academy of Sciences **105**, 1182 (2008).